magnetochemistry

MDPI

Perspective

Lanthanide-Based Metal–Organic Frameworks with Single-Molecule Magnet Properties †

Fabio Manna [1,2,3], Mariangela Oggianu [1,2], Narcis Avarvari [3,*] and Maria Laura Mercuri [1,2,*]

[1] Department of Chemical and Geological Sciences, University of Cagliari, Highway 554, Crossroads for Sestu, I-09042 Monserrato, Italy; f.manna@etud.univ-angers.fr (F.M.); mariangela.oggianu@unica.it (M.O.)
[2] National Interuniversity Consortium of Materials Science and Technology, INSTM, Street Giuseppe Giusti, 9, I-50121 Florence, Italy
[3] CNRS, MOLTECH-Anjou, SFR MATRIX University of Angers, F-49000 Angers, France
* Correspondence: narcis.avarvari@univ-angers.fr (N.A.); mercuri@unica.it (M.L.M.); Tel.: +33-241-735-084 (N.A.); +39-070-6754-474 (M.L.M.)
† Dedicated to Professor Manuel Almeida on the Occasion of His 70th Birthday.

Abstract: Lanthanide metal–organic frameworks (Ln-MOFs) showing single-molecule magnet (SMM) properties are an ever-growing family of materials where the magnetic properties can be tuned by various interrelated parameters, such as the coordinated solvent, temperature, organic linkers, lanthanide ions and their coordination environment. An overview of the general synthetic methodologies to access MOFs/Ln-MOFs and the peculiarities and parameters to control and/or fine-tune their SMM behavior is herein presented. Additionally, diverse challenging strategies for inducing SMM/SIM behavior in an Ln-MOF are discussed, involving redox activity and chirality. Furthermore, intriguing physical phenomena such as the CISS effect and CPL are also highlighted.

Keywords: lanthanide metal–organic frameworks; single-molecule magnets; single-ion magnets

Citation: Manna, F.; Oggianu, M.; Avarvari, N.; Mercuri, M.L. Lanthanide-Based Metal–Organic Frameworks with Single-Molecule Magnet Properties. *Magnetochemistry* **2023**, *9*, 190. https://doi.org/10.3390/magnetochemistry9070190

Academic Editors: Laura C. J. Pereira and Dulce Belo

Received: 27 June 2023
Revised: 17 July 2023
Accepted: 19 July 2023
Published: 22 July 2023

1. Introduction

Metal–organic frameworks (MOFs), crystalline porous materials formed by the self-assembling of metal ions (nodes) with organic ligands (linkers) [1–3], are attracting considerable interest in material science given their fascinating architectures, which can be tailored by a proper chemical design of linkers and nodes, and the richness of their chemical and physical properties [4–6], which make them promising platforms in a *plethora* of applications such as fuel storage, CO_2 capture, drug delivery, sensing and catalysis [7–9]. As far as magnetic MOFs are concerned, those exhibiting molecular properties, i.e., single-molecule magnets (SMMs), have attracted extensive attention in the field of chemistry, physics and material science due to their potential applications in cutting-edge molecular spintronics and quantum computing devices [10]. SMMs are fascinating materials [11] that have been continuously investigated since the first discovery of $Mn_{12}O_{12}(OAc)_{16}(H_2O)_4$ (known as Mn_{12}) by Sessoli et al. and the synthesis of the first Ln^{III}–SMM complex based on Dy^{III} [12–14]. The SMM efficiency is evaluated by three different parameters: (i) the blocking temperature (T_B), i.e., the highest temperature at which the magnetization is preserved during a given period of time [15]; (ii) the coercive magnetic field (H_c), described as the magnetic field needed to turn to zero the magnetization of an SMM; and (iii) the effective energy barrier (U_{eff}), the most used parameter, which indicates the energy required to convert an SMM into a paramagnet.

Although reported in the literature are many examples of magnetic MOFs, very few show SMM behavior [16]. On the other hand, porosity, the intrinsic property of MOFs, is typically favored by the use of long linkers, i.e., linkers bearing bulky pendant arms, whereas magnetic interactions require short distances between the metal nodes [17]. Thus, the chemical design of MOF-based SMMs is a challenging aspect, and, among the synthetic

strategies envisaged to develop MOF-based SMMs with efficient T_B, H_c and U_{eff} values, the use of Ln^{III} ions with large magnetic anisotropy occupies a prominent place.

Indeed, lanthanide-based MOFs (Ln–MOFs) are a class of porous materials that have attracted great interest during the last few decades thanks to their intrinsic advantages such as lanthanide coordination versatility and a wide range of applications due to their unique properties based on f-electrons offering the possibility to combine both luminescent centers and magnetic properties in the same crystal lattice, building up multifunctionality [18]. Lanthanides' valence electrons are located in 4f orbitals, which are shielded from the ligand field by fully filled $5s^2$ and $5p^6$ orbitals. For this reason, the 4f orbitals do not split due to weak interactions between the ligands and the orbitals, and the coordination environment around the 4f ion remains almost unaltered, giving rise to strong spin–orbit coupling interactions. The most used Ln^{III} ions to fabricate SMMs are Tb^{III}, Dy^{III}, Er^{III} and Ho^{III}. Particularly, Tb^{III} and Dy^{III} are the best candidates, since their electronic structure exhibits large magnetic anisotropy due to the strong angular dependence of 4f orbitals [19].

Recently a second generation of SMM-based MOFs, known as single-ion magnet (SIM) MOFs, started to rapidly develop since the first report of the $Ln(bipyNO)_4(TfO)_3$ (bipyNO = 4,40-bypyridyl-N,N0-dioxide, TfO = triflate) 3D coordination framework by Espallargas et al. [20] (*vide infra*). SIMs consist of single centers that exhibit slow magnetic relaxation [10], and, consequently, SIM-MOFs are formed by ordered assemblies of lanthanide ions and different bridging linkers, featuring extended and porous high-dimensional frameworks with tunable magnetic properties.

The present work aims to provide an overview, through selected examples, of the different strategies currently employed to integrate SMM/SIM functionality into an MOF. The MOF framework is then used as a suitable scaffold to constrain or tune the local geometries of lanthanide nodes (ions or clusters) and arrange diverse organic linkers into ordered assemblies, featuring a combination of structural diversity and SMM/SIM behavior. In this context, conventional and/or unconventional synthetic approaches toward SMMs/SIMs are also exploited.

2. Synthetic Methodologies

MOFs in general and Ln-MOFs in particular are conventionally obtained by combining organic linkers and metal ions via solvothermal and slow diffusion reactions (layering). Recently, other synthetic strategies have been explored as microwave-assisted, electrochemical, mechanochemical or sonochemical methods, as reported in Scheme 1. The final product is often obtained in the form of single crystals, suitable for X-ray structural studies, microcrystalline powders, nanocrystals or films [21]. Solvothermal synthesis is the most used technique to develop crystalline MOFs and consists of a combination of linkers and metal salts in a closed autoclave, heated under autogenous pressure. The crystal size and morphology are strongly influenced by several parameters, such as the solvent, temperature, concentration, pH, reaction time, etc. The major advantages are the control of the reaction conditions and the obtainment of single crystals suitable for structural characterization. The diffusion method consists of a slow mixing of metal salts and linker solutions by layering one on top of the other, taking advantage of their different densities. This technique is particularly useful for growing single crystals suitable for structural analysis. In the microwave-assisted method, the reactor is heated by electromagnetic waves. The parameters that influence the size and morphologies of the final product are similar to the solvothermal one, but the major advantages are low reaction time, energy saving and microcrystalline materials. In the mechanochemical methods, reactions between metal salts and linkers occur under high-speed grinding in a ball mill at ambient pressure. Metal oxides are frequently employed as starting precursors, and the crystallinity of the final product is generally low, but it could be improved by using different precursors or by adding a small amount of solvent. This method is economical and eco-friendly and very few or no solvents are used, but it affords poor crystalline final products. The electrochemical method is used for the synthesis of MOF thin films (from nano to microscale) whose morphologies could be

finely tuned by changing the electrosynthesis parameters (e.g., electrolytes, current density, additives and reaction time). This technique has in principle several advantages over the aforementioned methodologies, such as high-purity products, mild conditions and the facile control of film features, but in the case of Ln-MOFs, it may suffer from a reduction of Ln^{III} ions on the cathode during the process. In the sonochemical method, MOF synthesis occurs at room temperature by the application of high-energy ultrasound to a reaction mixture; this method is easy, rapid, environmentally friendly and allows for the obtainment of nanoscale MOFs with high crystallinity and different morphologies [22,23].

Scheme 1. Survey of synthetic methods.

The strategies to obtain high-temperature SMM-based Ln-MOFs are almost the same as for their molecular counterpart, and they could be summarized as follows: (i) make a proper choice of the crystal field for the Ln^{III} metal ion, taking into account its axial anisotropy; (ii) conduct large crystal field splitting by choosing the proper ligand field, whose shape should match the electronic density of the free metal ions [11,24,25]; (iii) commence strong magnetic interaction between the Ln^{III} ions, induced by the proper choice of diamagnetic or radical paramagnetic bridging ligands; and (iv) use isotopic Ln^{III} ions to suppress the hyperfine coupling, which favors the quantum tunnel of the magnetization relaxation process [26].

Furthermore, Ln-MOFs/coordination polymers (CPs) could be post-modified by external stimuli, such as (i) solvato-switching, principally due to the change in the coordination environment after solvent exchange or removal; (ii) photo-switching, through a mechanism where a change in the ligand with photochromic moieties is observed after irradiation, which could affect Ln-Ln distances and/or the coordination environment; (iii) redox-switching, through post-reduction/oxidation of the linker affording open-shell species, which could affect the exchange interactions of Ln^{III} ions, and also through a change in the open-shell species shape; and (iv) metal-ion exchange, where the incorporation of Ln^{III} ions in a preformed MOF framework occurs via exchange with a suitable cation, as reported by Pardo et al. [27]. Here, Ca^{II} ions could be exchanged by different Ln^{III} ions (Ln^{III} = Dy, Ho, Er) and NO_3^-, for charge compensation, inside the preformed MOF (*vide infra*). Recently, Long et al. reported on the use of mixed-valence $Dy^{II/III}$ ions in a dinuclear complex affording strong magnetic exchange interactions due to M–M bond formation and, consequently, high U_{eff} [28]; moreover, it has been reported that magnetic exchange

between Dy^{III} ions could be enhanced through the presence of soft donors, leading to excellent SMM behavior with high U_{eff} [14,29].

The post-modification (*vide supra*) of Ln-SMM-MOFs/CPs [27,30] occurred, in some cases, via an interesting on/off mechanism, particularly suitable for data manipulation applications, while in other cases, it led to a change in the SMM behavior, but in both cases, particular attention should be devoted to the reversibility of the process [31–33].

As highlighted by Powell et al. [34], another promising synthetic strategy is the use of a secondary building unit (SBU) acting as an SMM center, which can govern coordination numbers and the local geometry of the metal nodes of the assemblies in 2D/3D frameworks. Indeed, MOFs have ordered arrangement of SMMs units, one of the most significant advantages with respect to their molecular counterpart [18,34]. For example, Murugesu et al. reported on a binuclear complex $[Dy_2(hmi)_2(NO_3)_2(MeOH)_2]$ (H_2hmi = 2-hydroxy-3-methoxyphenyl methylene (isonicotino)hydrazine) exhibiting SMMs, which could form a 2D network due to the coordination of Dy^{III} ions to the peripheral pyridyl N atoms of the linker. The 2D framework $[Dy_2(hmi)_2(NO_3)_2(MeOH)_2]n_\infty$ MeCN shows remarkably higher U_{eff} than the binuclear complex [35,36].

3. Single-Molecule Magnet/Ion-Based Ln-MOFs (SMM/SIM-MOFs)

The use of MOFs as a rigid platform (*vide supra*) to constrain and chemically tune the coordination geometries of lanthanide nodes, featuring high coordination numbers, has been shown to be a straightforward strategy for the rational control of SMM behavior, as demonstrated by a proper change in the synthetic conditions (nature of the solvents, temperature, etc., *vide infra*).

The solvent can play a crucial role in determining the supramolecular architecture, as reported by Cheng et al. [37]. Two different MOFs, formulated as $\{[Dy_2(FDA)_3(DMF)_2]\cdot 1.5DMF\}_n$ (**1**) and $[Dy_2(FDA)_3(DMF)_2(CH_3OH)]_n$ (**2**) (H_2FDA=furan-dicarboxylic acid, see Chart 1), have been obtained, where the use of the DMF/CH_3OH) solvent mixture leads to a moderate distortion of the Dy^{III} ions coordination sphere in **2** from an ideal D_{4d} with respect to **1**, resulting in a considerable improvement of the SMM behavior (Figure 1). Theoretical calculations demonstrated that Dy^{III} ions in **1** and **2** MOFs exhibit biaugmented trigonal-prismatic geometries (C_{2v}), and the estimated (calculated) deviation parameters are 1.579 (4.076) and 0.671 (1.786) for **1** and **2**, respectively, supporting the observed moderate deviation from an ideal D_{4d} symmetry in the latter than in the former. Because of the occupancy of the two coordinated solvents, the FDA^{2-} ligands in **2** adopt a μ_2-η_1:η_1-bridging coordination mode, resulting in a less distorted DyO_8 polyhedron of D_{4d} symmetry. When methanol was removed from **2**, a different MOF, formulated as $\{[Dy_2(FDA)_3(DMF)_2]\cdot 2.2DMF\}$ (**1′**), was obtained, where a seven-coordinate Dy^{III} ion is present, surrounded by six carboxylic oxygen atoms and one DMF molecule. The Dy^{III} ion shows a monocapped triangular-prismatic C_{2v} geometry, and a three-dimensional *stp* topological framework is constructed by connecting, via FDA^{2-} ligands, Dy^{III} ions into one-dimensional chains. Remarkably **1′** does not show slow relaxation of magnetization, highlighting the role played by the lanthanide coordination geometry in tuning the SMM behavior. Furthermore, the corresponding **1**@Y and **2**@Y, diluted by diamagnetic Y(III) ions, which should reduce or eliminate magnetic interactions between dysprosium(III) ions, show similar SMM behavior as the pristine **1** and **2** MOFs, confirming that magnetization relaxation depends on the Dy(III) ions' crystal field induced by the observed moderate deviation from the ideal D_{4d} geometry.

The temperature can also induce a fine-tuning of the coordination geometry of lanthanide ions in Ln-MOFs, which can significantly influence the SMM properties, also providing insights into the magneto-structural relationship. Cheng et al. reported on $[Dy_3(OBA)_4(HCOO)(H_2O)(DMF)]_n$ (**3**) and $[Dy(OBA)(HOBA)(H_2O)_2]\cdot 3DMF\}_n$ (**4**) (H_2OBA = 4,4′-oxybis(benzoate)acid) Ln-MOFs, obtained by reacting $Dy(NO_3)_3\cdot 6H_2O$ with H_2OBA for 3 days at 160 °C (**3**, orthorhombic, $C_{mc}2_1$ space group) and 80 °C (**4**, triclinic space group P1). Interestingly, **3** undergoes a reversible structural transformation to **4** by standing in its mother liquor for two days at room temperature and vice versa by heating **4** in its mother liquor up to 120 °C for 3 days. This process, ther-

mally induced, provokes a dramatic change in SMM properties, leading to switchable "ON/OFF" SMM behavior due to a significant change in the coordination geometries of the Dy^{III} ion from the C_{2v}/C_{4v} in **3** (paramagnet) to D_{4d} symmetry in **4** (SMM) because of a variation of its coordination mode.

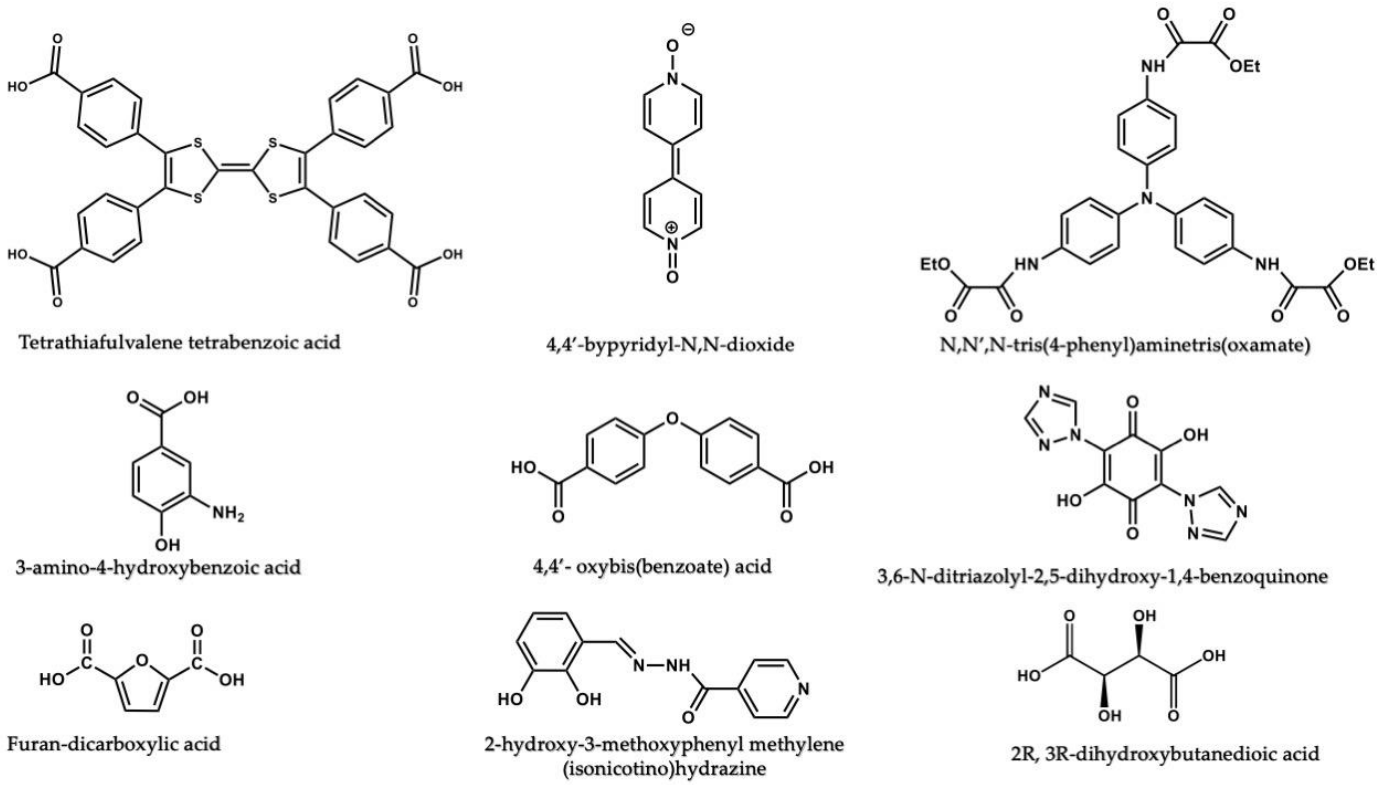

Chart 1. Organic linkers reported in Section 3.

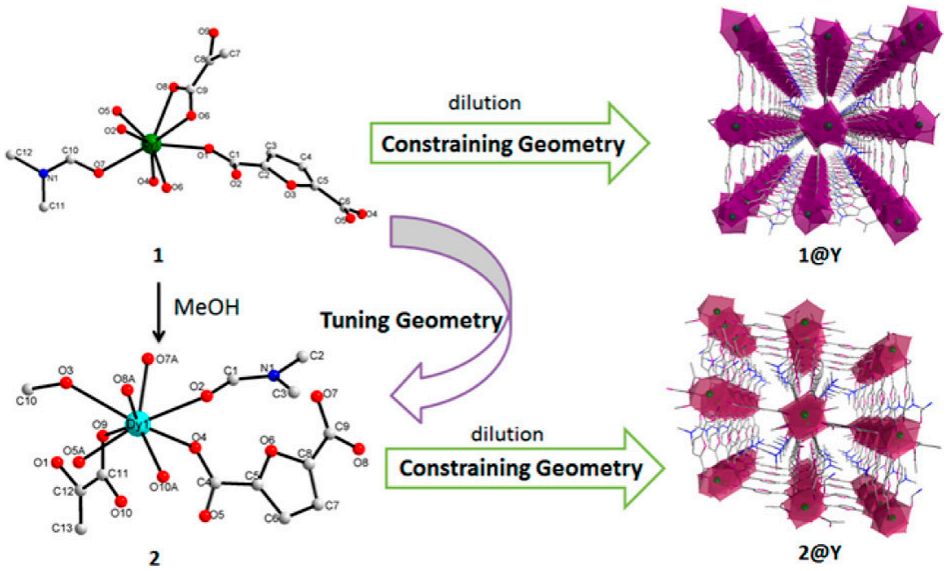

Figure 1. Constraining and Tuning the Local Geometries of Lanthanide Ions in Dy MOFs **1** and **2**. Reprinted with permission from [37].

The study of the mechanism of the structural conversion process from **4** to **3** evidenced the crucial role of temperature in constructing the 3D framework, breaking inter-layer $\pi\cdots\pi$ stacking interactions and hydrogen bonds and leading to the coordination environment around the Dy^{III} ion of C_{2v}/C_{4v} symmetry, observed in **3**, as shown in Figure 2 [38].

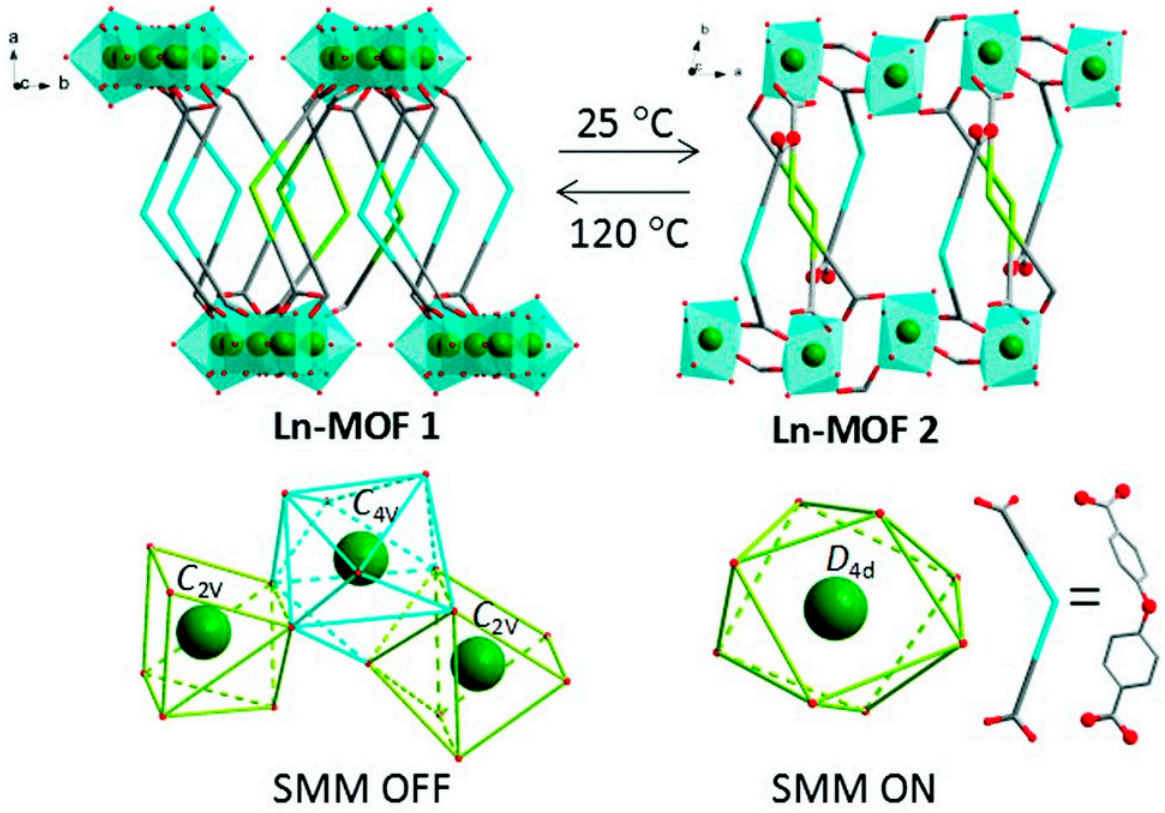

Figure 2. Schematic representation of reversible **3**→**4** structural transformation (**top**). Dy(III) ions' coordination symmetries and their related "ON/OFF" switching of magnetization relaxation in a zero *dc* field (**bottom**). Reprinted with permission from Ref. [38].

The careful choice of lanthanide nodes with a proper coordination environment is also a challenging strategy to construct an MOF with SMM properties. Particularly, mononuclear lanthanide complexes, where the first coordination sphere consists of the Ln^{III} ion surrounded by hard atoms (O, N) in a square-antiprismatic geometry, which is shown to favor SIM behavior, are promising candidates, as reported by Coronado et al. [20] through the novel family of Ln-MOFs formulated as $[Ln(bipyNO)_4](TfO)_3 \cdot x$ solvent (Ln=Tb (**5**); Dy (**6**); Ho (**7**); Er (**8**); and bipyNO= 4,4′-bypyridyl-N,N-dioxide, TfO = triflate]. The choice of the linker is very important as well, as long linkers (*vide supra*), such as bipyNO, are preferred since they are capable of keeping lanthanide centers isolated and reducing dipole interactions.

These 3D Ln-MOFs exhibit slow magnetic relaxation, behaving as SIM-MOFs, as confirmed by magnetic measurements (Figure 3).

Interestingly, the incorporation of large anions as polyoxometalates (POMs), particularly $[Mo_6O_{19}]^{2-}$ polyanions, reported in Figure 4, does not affect the magnetic behavior, and retainment of slow magnetic relaxation is observed, despite the exchange with triflate anions. This is due to the preservation of the structural features of the 3D framework, despite the sterically hindered POM anions, which are located in the cavity of MOFs but far from the lanthanide centers. These findings further demonstrate that SIM behavior is strictly related to the lanthanide coordination geometry and also pave the way to introduce non-innocent POM anions into multifunctional SIM-MOFs or to use POM-MOFs, which are materials with very large surface areas and thus potential candidates for applications in heterogeneous catalysis, where large porosity is required [20].

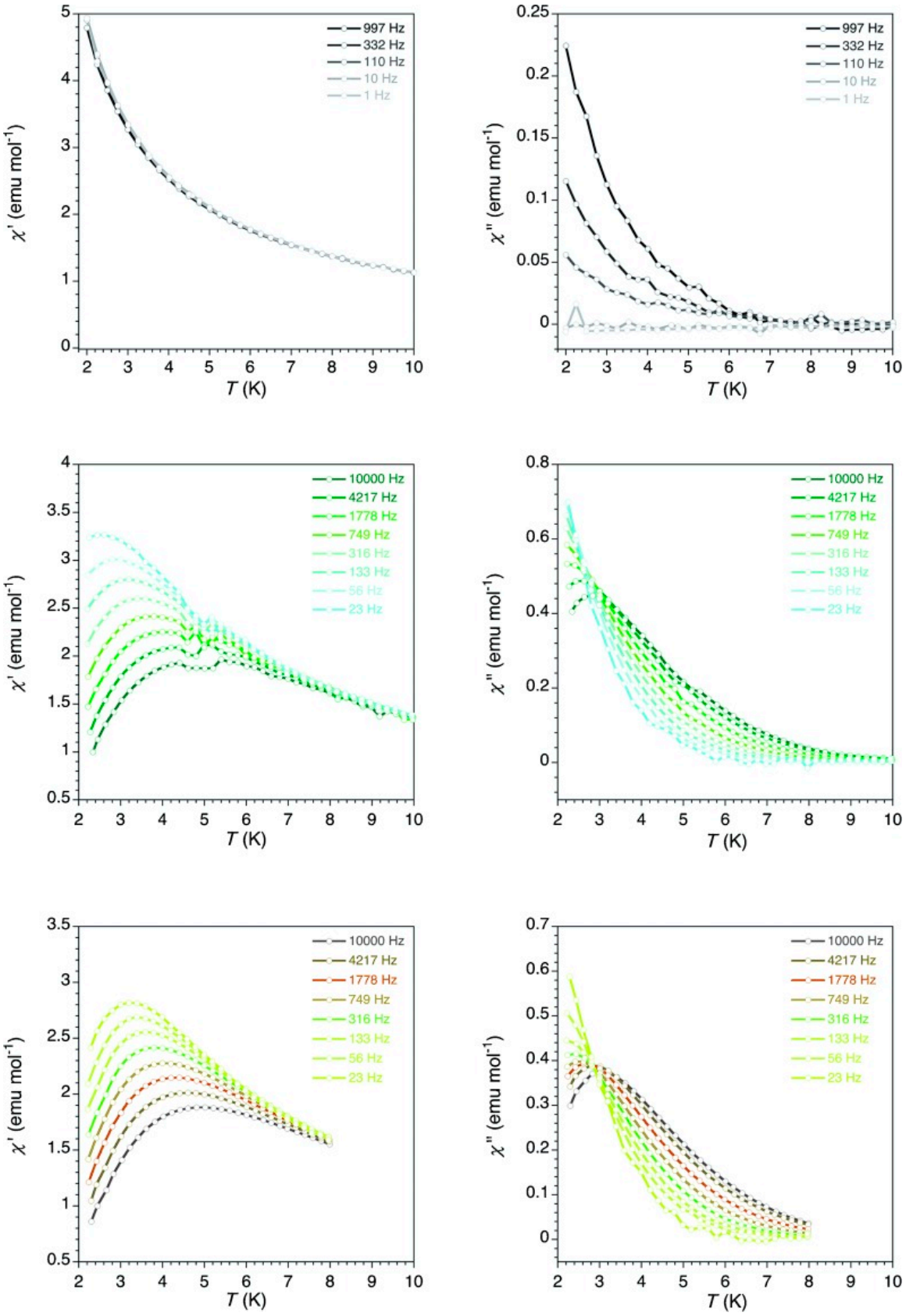

Figure 3. Dynamic susceptibility of **6**: left, in-phase; right, out-of-phase, in applied dc magnetic fields; and 0 G (top) and 1000 G (bottom). Adapted with permission from [20].

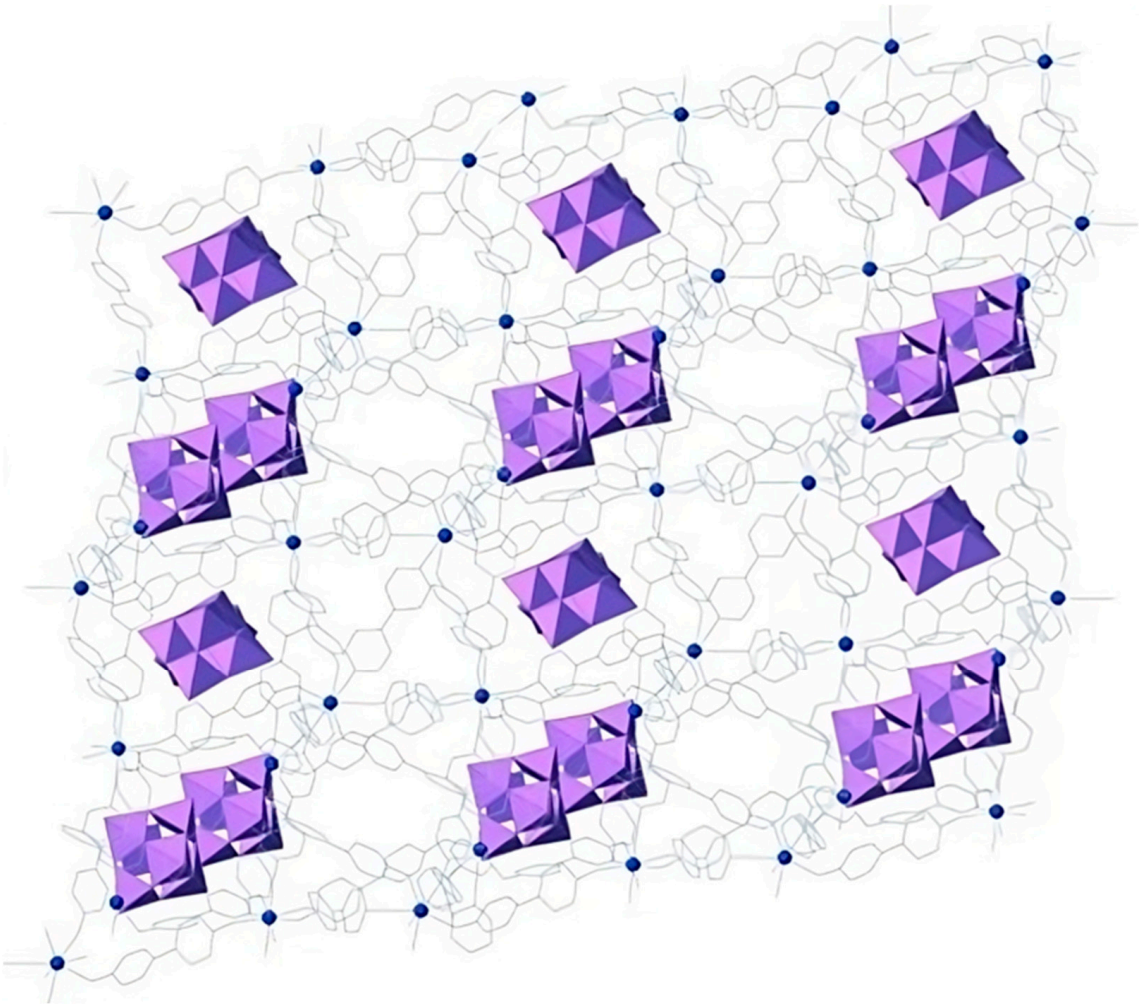

Figure 4. Crystal structure of **6**-POM, with POMs (purple) in the cavities. Dy atoms and bipyNO linkers are in blue and grey, respectively. Reprinted with permission from [20].

The combination of post-synthetic methodologies (PSMs) with the molecular approach, consisting of the use of metal complexes as suitable linkers toward selected metal nodes, is a powerful strategy for governing the structure of SMM-MOFs and tuning their magnetic properties through a fine modulation of their structural characteristics. In fact, it has been shown that small structural changes in the coordination geometry of the lanthanide ion in an SMM-MOF provoke significant changes in its magnetic behavior. Pardo et al. [27] reported on the use of an oxamato-based tetranuclear Co^{III} complex as a suitable building block toward Ca^{II} metal ions to construct a diamagnetic Ca^{II}-Co^{III} 3D MOF, formulated as $\{Ca^{II}_6(H_2O)_{24}[Co^{III}_4(tpatox)_4]\}\cdot 44H_2O$ (**9**), ($tpatox^{6-}$ = N,N′,N-tris(4-phenyl)aminetris(oxamate)). Interestingly, the oxamate-based complex is formed by tetrahedral cages obtained by combining a multitopic linker, the bulky tripodal tpatox ligand (N,N,N-tris(4-phenyl)aminetris(oxamate), with Co^{III} ions. When the metal-ion exchange post-synthetic method is used, by replacing Ca^{II} ions with Tb^{III}, Dy^{III}, Ho^{III} and Er^{III} ions, isostructural Ln^{III}–Co^{III} 3D MOFs formulated as $\{[Tb^{III}_6(H_2O)_{24}[Co^{III}_4(tpatox)_4]](NO_3)_6\}\cdot 49H_2O$ (**10**), $\{[Dy^{III}_6(H_2O)_{24}[Co^{III}_4(tpatox)_4]](NO_3)_6\}\cdot 53H_2O$ (**11**), $\{[Ho^{III}_6(H_2O)_{30}[Co^{III}_4(tpatox)_4]](NO_3)_6\}\cdot 44H_2O$ (**12**) and $\{[Er^{III}_6(H_2O)_{24}[Co^{III}_4(tpatox)_4]](NO_3)_6\}\cdot 58H_2O$ (**13**) are obtained through a single-crystal-to-single-crystal solid-state process (Figure 5). It is noteworthy that **11** and **13** MOFs, containing Kramers' ions as metal nodes, exhibit slow relaxation of

magnetization, thus behaving as SIM-MOFs, while the one-pot reaction between the related $Na_{12}[Co^{III}_4(tpatox)_4]\cdot 6H_2O$ and $Ln(NO_3)_3\cdot {}_5H_2O$ salts did not afford **10–13**. The crucial role of post-synthetic and molecular approaches to construct MOFs with SIM properties is therefore evidenced.

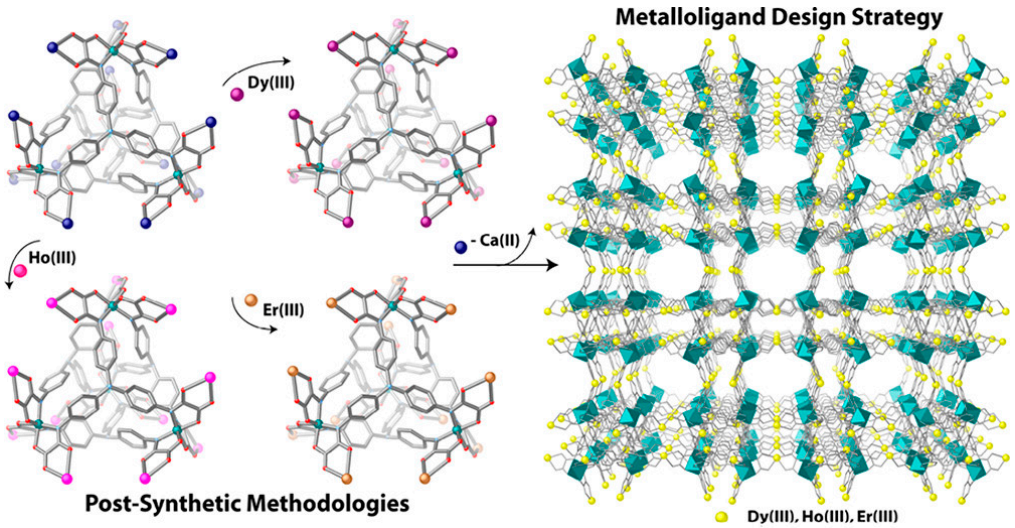

Figure 5. Perspective views of $([Co_4(tpatox)_4]^{12-}$ tetrahedral cages containing Ca^{II} or Dy^{III}, Ho^{III} and Er^{III} exchanged by post-synthetic methods, as building blocks of isostructural **10–13** MOFs (**left**); **9** MOF, along the *a* crystallographic axis (**right**). Co^{III} and Ca^{II} metal ions and linkers are in gray, cyano and blue, respectively. Reprinted with permission from [27].

It has been shown that the coordination geometry of lanthanide ions, in a rigid scaffold as an MOF, can significantly influence its SIM/SMM properties. It is noteworthy that in the case of flexible MOFs [39,40], flexibility may be due to a reversible dehydration/hydration process, when coordinated water molecules are present in the first coordination sphere of the Ln^{III} ion. As a consequence, a change in the coordination environment is observed, resulting in a significant modulation of the relaxation of the magnetization barrier. Very recently, some of us [40] reported on two multifunctional 3D polymorphic frameworks (**14a,b**), formulated as $[Er_2(trz_2An)_3(H_2O)_4]_n\cdot xH_2O$ (x = 10, **a**; x = 7, **b**), showing a combination of luminescent and magnetic properties, where **14a** is a 3D flexible MOF. These two polymorphs were obtained by combining the NIR-emitting Er^{III} ion with the 3,6-N-ditriazolyl-2,5-dihydroxy-1,4-benzoquinone (H_2trz_2An) linker, bearing bulky triazole-based pendant arms. Moreover, **14a** shows a reversible structural phase transition to a partially dehydrated 3D structure, formulated as $[Er_2(trz_2An)_3(H_2O)_2]_n\cdot 2H_2O$ **(14a_des; des = desolvated**), from ennea- to octa-coordination of the Er^{III} coordination geometry through a reversible loss of a water molecule, which occurred under vacuum or heating up 360 K. Remarkably, structural flexibility provokes the fine-tuning of both luminescent and SIM properties, involving a moderate change in NIR emission and a slight improvement of the magnetic blocking temperature in the dehydrated structural phase. The dehydration/hydration mechanism has been investigated by theoretical calculations, which evidenced that the observed improvement of magnetic properties is mainly due to the variation in the ligand field induced by the loss of the water molecule (Figure 6).

Redox activity has been demonstrated to be an efficient strategy for tuning the conducting and magnetic properties in MOFs due to the generation of organic radicals, which can improve magnetic exchange between metal nodes [4,40–42]. Redox-active linkers can affect also the SMM behavior; therefore, they can act as switchable nodes for constructing redox-controlled SMM-MOFs. Linkers based on a tetrathiafulvalene (TTF) *core*, which possess different oxidation states, such as radical $TTF^{\cdot+}$ and diamagnetic TTF^{2+} species, are efficient ON/OFF redox switches. Zhou et al. [32] have combined, via a solvothermal reaction, ennea-nuclear lanthanide clusters showing SMM behavior, as inorganic nodes, and

TTF-based linkers, as redox switches, to construct 3D SMM-MOFs. Interestingly, crystals of $Ln_9(\mu_3\text{-}OH)_{13}(\mu_3\text{-}O)(H_2O)_9(TTFTB)_3]$ (H_2TTFTB = tetrathiafulvalene tetrabenzoic acid)] were obtained with Ln^{III} = Dy (**15**), Tb (**16**) and Er (**17**). As an example, in **15**, each Dy_9 cluster is linked to $TTFTB^{4-}$ linkers through 12 carboxylate groups, which coordinate in a *syn-syn* bidentate mode, leading to a framework formed by 12-connected hexagonal prisms combined with 4-connected $TTFTB^{4-}$ linkers, which coordinate in a square planar manner, resulting in a shp-a topology (shp = square hexagonal prism) as reported in Figure 7a,b).

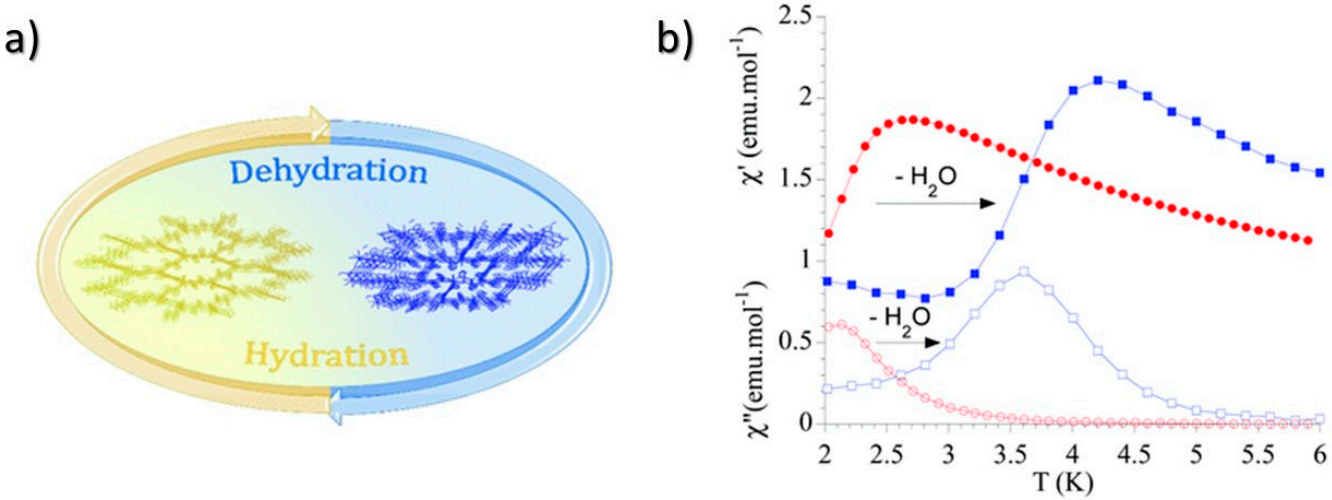

Figure 6. (**a**) Reversible expansion/shrinkage from hexagonal distorted cavities in **14a** to distorted 3,6-brickwall rectangular cavities in **14a_des** (**left**); (**b**) plot of χ' and χ''*vs* T of 14a(full and empty red circles, respectively and 14a_desfull and empty blue circles)) under an applied dc field of 0.09 T at 10,000 Hz. Adapted with permission from [40].

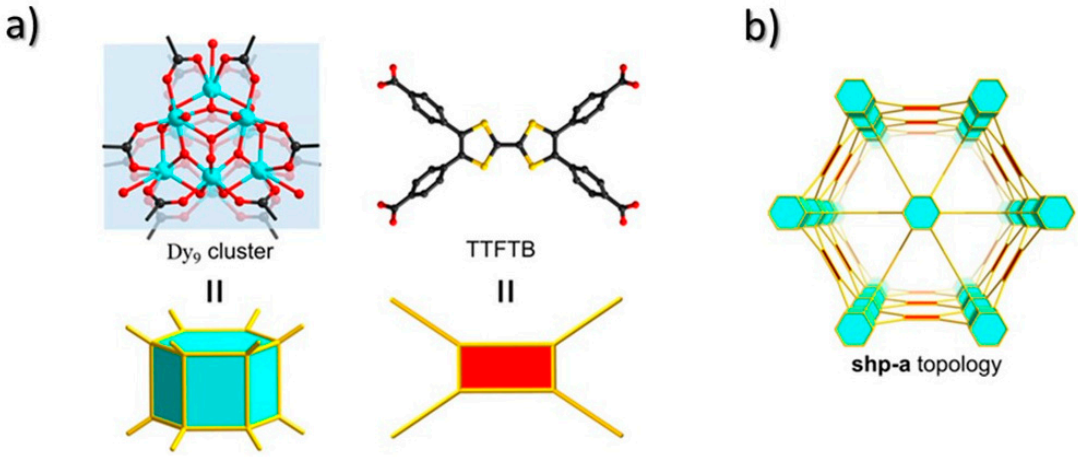

Figure 7. (**a**) The 12-connected Dy9 cluster and 4-connected TTFTB linker in a hexagonal prism and square planar coordination modes, respectively. (**b**) shp-a topology. Adapted with permission from [32].

Remarkably, these multifunctional MOFs, which are isostructural, possess, other than high porosity (Brunauer–Emmett–Teller surface areas of 1515, 1635 and 1800 $m^2 \cdot g^{-1}$ for **15**, **16** and **17,** respectively), redox activity and slow relaxation of magnetization, which can be switched OFF upon post-synthetic oxidation with I_2 of the TTFTB linker to its corresponding radical S = 1/2 cation and I_3^- anion or by solvent exchange of DMF (N, N-dimethylformamide) guest molecules with cyclohexane or I_3^- anions inside the cavities. Most importantly, this process is reversible, and the SMM behavior can be switched ON through a reduction in the DMF solution. Furthermore, structural features are also retained

in the corresponding oxidized MOFs. These promising results show that the fine-tuning of the SMM behavior via redox activity of the organic building blocks can provide a valuable way to control, through external stimuli and/or solvent exchange, the SMM properties of lanthanide clusters within a rigid platform as an MOF for future applications in functional devices based on redox-switchable and multi-stimuli responsive SMM-MOFs.

Very recently, Seco et al. [43] reported on a novel family of 3D magneto-luminescent Ln-MOFs, formulated as a $\{[Ln_5L_6(OH)_3(DMF)_3]\cdot_5H_2O\}_n$-based 3-amino-4-hydroxybenzoic acid linker (H_2L) and Ln^{III} ions (Nd, Sm, Eu, Gd, Tb, Dy, Ho, Er, Tm and Yb), including NIR emitters (Nd, Er and Yb). They are isostructural, and, most importantly, they are multifunctional, showing a combination of porosity, photoluminescence and SMM behavior. In particular, the latter is observed in Dy (**18**), Er (**19**) and Yb (**20**) MOFs due to the oblate or prolate character of lanthanide ions, which depend on the electronic distribution of the coordination geometry. Specifically, in oblate-type ions (Dy^{III}), magnetic anisotropy is enhanced by axially coordinated donor atoms of the linker, showing the highest electron density, while in prolate-type ions (Er^{III}, Yb^{III}), coordination at equatorial positions is preferred to induce greater magnetic anisotropy. Magnetic measurements on **18**–**20**, reported in Figure 8, evidence that no frequency dependence is present without applying an external field due to quantum tunneling of magnetization (QTM). Under a static field (1000 Oe), QTM is suppressed, and, interestingly, frequency dependence is observed only in **20**, which represents, *according to the authors*, the first 3D SMM-MOF containing NIR-emitting Yb^{III} ions, since Yb-MOFs are rare. Magnetic diluted yttrium-based MOFs were prepared to obtain insights on the magnetization relaxation process, and the magnetic studies evidence the crucial role of the electron density distribution, the prolate vs. oblate nature of lanthanide ions in tuning the magnetic anisotropy and thus the SMM properties. Photoluminescence studies on Eu/Tb-MOFs and their corresponding heterobimetallic MOFs (stoichiometric ratio 50:40:10/5) evidence the potential of the doped materials as ratiometric thermometers. Additionally, the microporous structure of these MOFs makes them potential candidates for CO_2 capture and separation, particularly Dy-MOF (**18**), which is the material showing the best performance in terms of sorption capacity.

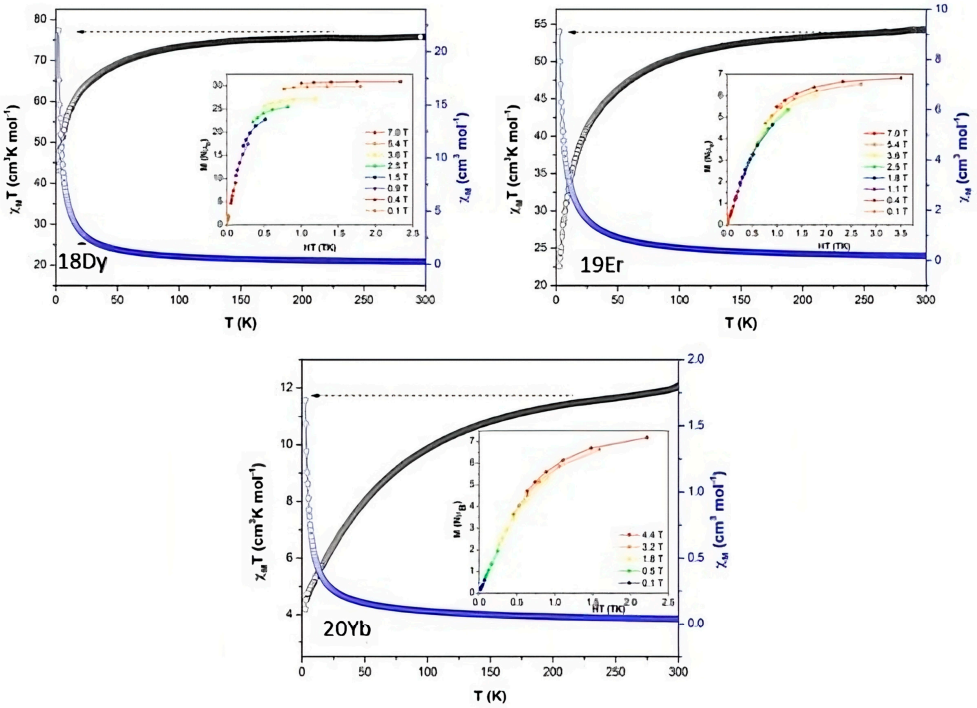

Figure 8. Thermal variation in $\chi_M T$ vs. T, under an applied field of 1000 Oe, for **18–20**. Adapted with permission from Ref. [43].

The use of chiral linkers in a hybrid platform as an MOF is a challenging strategy to study physical phenomena related to the interaction of chiral materials with a polarized electromagnetic field, such as circularly polarized luminescence (CPL) [44], the emission of circularly polarized light upon irradiation, which can have potential applications in optical data storage and spintronics [45]. Ln-MOFs are then promising candidates, since lanthanide(III) ions can boost the CPL performances [46], even though the studies on chiral Ln-MOFs, including those showing SMM behavior, are still scarce due to the difficulties of governing chirality in a hybrid framework. Cepeda et al. [47] reported on a new family of 3D chiral magneto-luminescent Ln-MOFs of formula $\{[Ln_2(\mu_4\text{-tar})_2(\mu\text{-tar})(H_2O)_2]\cdot 3H_2O\}_n$), with [$Ln^{III}$ = Tb, Dy, Ho, Er and Tm and x = 3 or 4, depending on the counteranion with the *D*- or *L*- tartrate (tar = 2R, 3R-dihydroxybutanedioate) chiral linker. These enantiomerically pure MOFs are all isostructural, thermally stable and flexible, showing different phases depending either on the ion size or the temperature variation, ranging from partially (Ln-L′ and Ln-L″) to fully (Ln-L‴) dehydrated structures. Magnetic studies show that Tb-, Dy- and Er-*L*-MOFs (**21**, **22** and **23**) exhibit SMM behavior upon application of an external field and discrete values of an energy barrier (U_{eff}) due to a residual QTM (in particular for Dy-MOF, **22**), which is suppressed through a magnetic dilution with yttrium(III) in the related yttrium-based MOFs, as reported in Figure 9. The dehydration/hydration process is reversible and, remarkably, modulates both the magnetic and photoluminescence responses.

Number **22**, which shows tunable SMM and luminescent properties, which depend on the dehydration/hydration process, has the potential to be used in humidity-sensing applications. Number **21** represents the second example of a chiral MOF showing the CPL property. In the CPL spectrum of **21**, reported in Figure 10, the emission assigned to the $^7F_5 \leftarrow {}^5D_4$ transition is split mainly into two bands, centered at 540 and 555 nm, due to the degeneration removal of sublevels induced by the environment chirality.

These two bands show opposite signs and luminescence dissymmetry factor values around 4×10^{-3}, which, although modest, are similar to those reported in the literature for terbium coordination polymers. Most importantly, **22** (Dy-*L*-MOF, *vide supra*) represents the first example, to the best of our knowledge, of a multifunctional chiral Ln-MOF showing chirality-induced spin selectivity (CISS) [48,49], the generation of a spin-polarized current by injecting electrons through a chiral material without the presence of a magnetic field. The first report on the performance of Dy-*L*-MOF as an almost ideal spin filter is made by San Sebastian et al. [50]. The impressive spin selectivity found is due to the 3D helicoidal packing pattern, which may boost the electronic conduction along the crystallographic axes through the helices. The CISS effect is also influenced by the large spin-orbit coupling of dysprosium (III) ions, which, along with the 3D helicity exhibited by this MOF, may be responsible for the observed remarkably high spin polarization values. In Figure 11, a schematic representation of the CISS effect is reported.

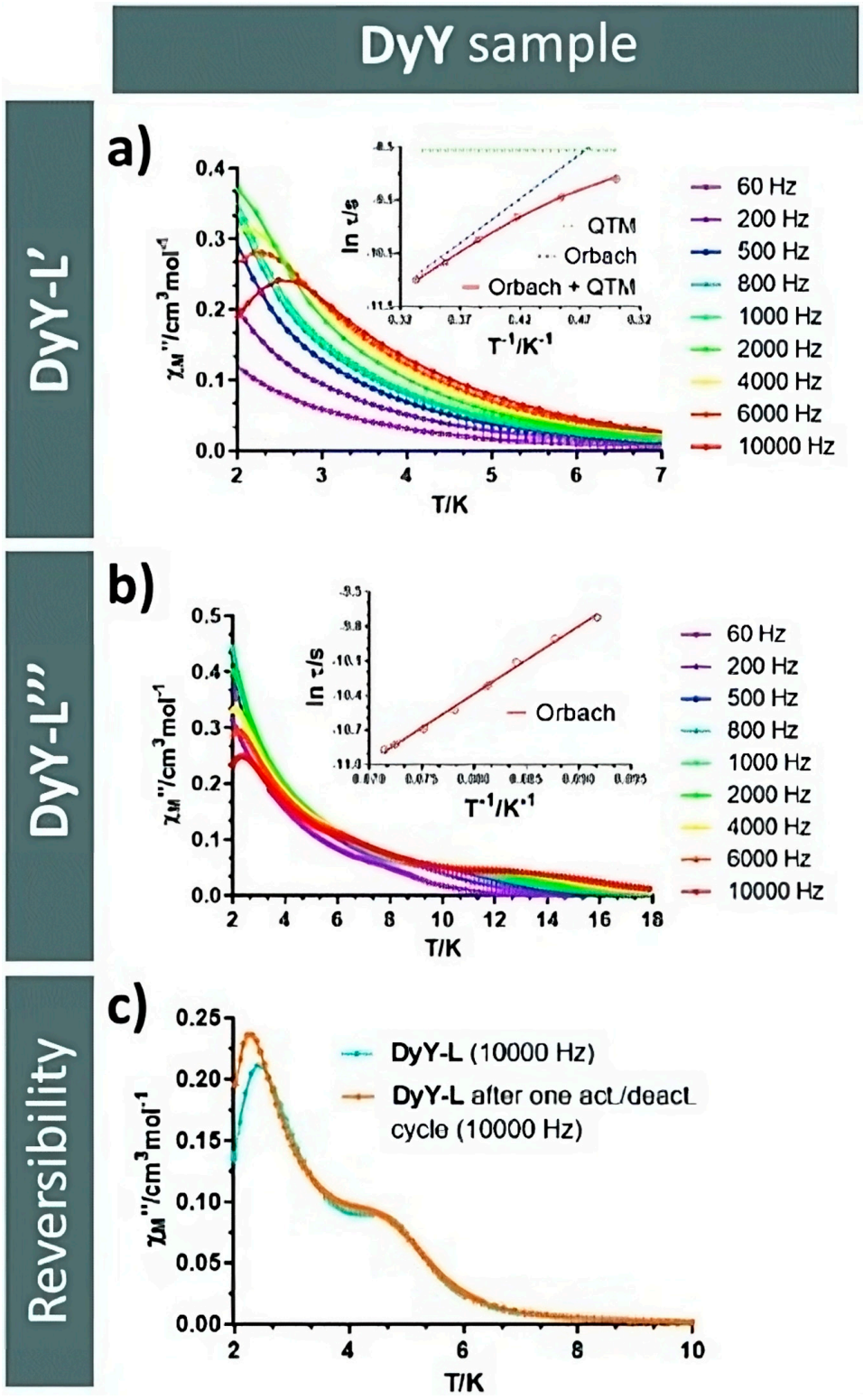

Figure 9. Thermal variation in out-of-phase $\chi_M T$ vs. T, under an applied field of 1000 Oe, for **22**, partially (**a**) and completely (**b**) dehydrated. Insets: Relaxation times vs. T and related best fits. (**c**) ac curves at 10,000 Hz for **22**, non-activated and completely dehydrated/rehydrated. Adapted with permissions from Ref. [47].

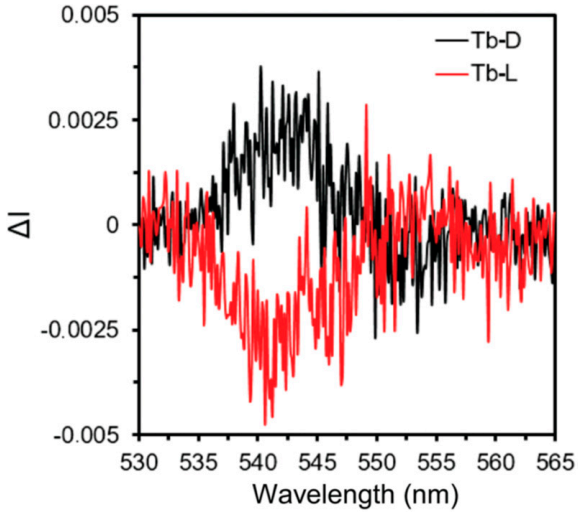

Figure 10. CPL spectra centered at the $^{7}F_{5}\leftarrow{}^{5}D_{4}$ transition of **21** (Tb-L and Tb-D). Reprinted with permissions from Ref. [47].

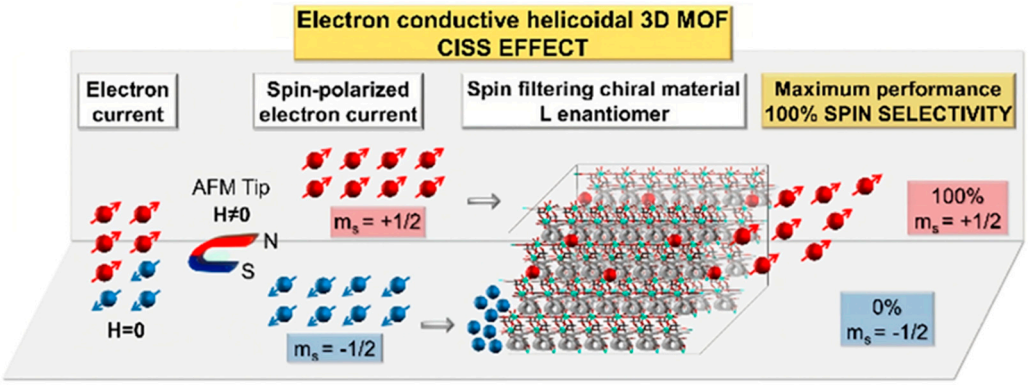

Figure 11. Schematic representation of the CISS effect in a helicoidal 3D MOF (**22**). Reprinted with permission from [50].

4. Summary and Outlook

Ln- MOFs have been demonstrated to be suitable platforms for the rational control of SMM behavior by the fine modulation of different parameters, such as synthetic protocols, involving temperature and the nature of the solvents, a careful choice of linkers and metal nodes, including preformed SMMs, and, most importantly, the coordination geometry, involving a rigid or flexible scaffold. The use of redox-active linkers has been shown to be a challenging strategy for achieving the fine-tuning of the SMM behavior through external stimuli and/or solvent exchange in redox-switchable and multi-stimuli-responsive SMM-MOFs. On the other hand, chiral linkers allow for exploiting physical phenomena such as CPL [44] and the CISS effect, observed for the first time in a 3D helicoidal Dy-MOF, which showed unprecedented spin polarization values. In this *scenario*, the combination of porosity with SMM and luminescent properties offers a route to building up multifunctionality as a powerful tool to further tune these properties through intermolecular interactions between guest molecules present in the pores and the 3D framework. It should be highlighted that a rational design of high-performance SMMs/SIMs, with improved energy barriers for the magnetization reversal, requires a careful choice of the coordination environment of lanthanide ions in terms of the ligand field. With this view, the linker donor atoms possessing high electron density should coordinate oblate Ln^{III} ions (Dy and Tb) at the axial positions, while prolate ions (Er and Yb) should be coordinated at the equatorial positions, in or-

der to maximize their anisotropic electron density *(vide supra)*. As perspectives, the use of soft linkers, unexplored in the SMM-MOF field probably due to the hard character of the Ln^{III} ions, can be challenging due to the occurrence of strong exchange interactions observed in their molecular counterpart, a binuclear Dy^{III} complex bridged by sulfur atoms [29]. Furthermore, paramagnetic radical linkers should be developed, since these open-shell ligands have the potential to mediate strong magnetic interactions unless Ln^{III} centers bridged by these ligands exhibit short distances [51]. A further achievement is represented by photo-switchable MOFs, not reported up to now, since a change in magnetic properties with light could be promising in the construction of spintronic devices. In conclusion, these relevant findings pave the way to construct next-generation materials with improved performances for optical data storage and spintronic applications.

Author Contributions: N.A. and M.L.M. defined the topic and the main content of the review. F.M. and M.O. equally wrote parts of the initial draft, supervised, reviewed and completed by N.A. and M.L.M. All authors have read and agreed to the published version of the manuscript.

Funding: This research was funded in Italy by the Fondazione di Sardegna, Convenzione triennale tra la Fondazione di Sardegna e gli Atenei Sardi, Regione Sardegna, L.R. 7/2007 annualità 2020, through the SMAWRT project (CUP F75F21001260007).

Institutional Review Board Statement: Not applicable.

Informed Consent Statement: Not applicable.

Data Availability Statement: Not applicable.

Acknowledgments: The SMAWRT project (CUP F75F21001260007) is acknowledged for M.O.'s post-doctoral grant. The MUR (Ministry of Education, University, Research) and UNICA-UNISS Consortium PhD Course on Chemical Sciences and Technologies are also acknowledged for F.M.'s Ph.D. grant. The work in France was supported by the CNRS and the University of Angers.

Conflicts of Interest: The authors declare no conflict of interest. The funders had no role in the design of the study; in the writing of the manuscript; or in the decision to publish the results.

References

1. O'keeffe, M. Design of MOFs and intellectual content in reticular chemistry: A personal view. *Chem. Soc. Rev.* **2009**, *38*, 1215–1217. [CrossRef]
2. Yazaydin, A.Ö.; Snurr, R.Q.; Park, T.H.; Koh, K.; Liu, J.; LeVan, M.D.; Benin, A.I.; Jakubczak, P.; Lanuza, M.; Galloway, D.B.; et al. Screening of metal-organic frameworks for carbon dioxide capture from flue gas using a combined experimental and modeling approach. *J. Am. Chem. Soc.* **2009**, *131*, 18198–18199. [CrossRef] [PubMed]
3. Yaghi, O.M.; Li, G. Li Hailian Yaghi-Selective binding and removal of guests in a imcroporous metal-organic framework-Nature 1985. *Nature* **1995**, *378*, 703–706. [CrossRef]
4. Monni, N.; Oggianu, M.; Sahadevan, S.A.; Mercuri, M.L. Redox activity as a powerful strategy to tune magnetic and/or conducting properties in benzoquinone-based metal-organic frameworks. *Magnetochemistry* **2021**, *7*, 109. [CrossRef]
5. Sahadevan, S.A.; Abhervé, A.; Monni, N.; De Pipaón, C.S.; Galán-Mascarós, J.R.; Waerenborgh, J.C.; Vieira, B.J.C.; Auban-Senzier, P.; Pillet, S.; Bendeif, E.E.; et al. Conducting Anilate-Based Mixed-Valence Fe(II)Fe(III) Coordination Polymer: Small-Polaron Hopping Model for Oxalate-Type Fe(II)Fe(III) 2D Networks. *J. Am. Chem. Soc.* **2018**, *140*, 12611–12621. [CrossRef] [PubMed]
6. Sahadevan, S.A.; Monni, N.; Abhervé, A.; Marongiu, D.; Sarritzu, V.; Sestu, N.; Saba, M.; Mura, A.; Bongiovanni, G.; Cannas, C.; et al. Nanosheets of Two-Dimensional Neutral Coordination Polymers Based on Near-Infrared-Emitting Lanthanides and a Chlorocyananilate Ligand. *Chem. Mater.* **2018**, *30*, 6575–6586. [CrossRef]
7. Monni, N.; Andres-Garcia, E.; Caamaño, K.; García-López, V.; Clemente-Juan, J.M.; Giménez-Marqués, M.; Oggianu, M.; Cadoni, E.; Espallargas, G.M.; Clemente-León, M.; et al. A thermally/chemically robust and easily regenerable anilato-based ultramicroporous 3D MOF for CO2uptake and separation. *J. Mater. Chem. A* **2021**, *9*, 25189–25195. [CrossRef]
8. Oggianu, M.; Monni, N.; Mameli, V.; Cannas, C.; Sahadevan, S.A.; Mercuri, M.L. Designing magnetic nanomofs for biomedicine: Current trends and applications. *Magnetochemistry* **2020**, *6*, 39. [CrossRef]
9. Sahadevan, S.A.; Monni, N.; Oggianu, M.; Abhervé, A.; Marongiu, D.; Saba, M.; Mura, A.; Bongiovanni, G.; Mameli, V.; Cannas, C.; et al. Heteroleptic NIR-Emitting YbIII/Anilate-Based Neutral Coordination Polymer Nanosheets for Solvent Sensing. *ACS Appl. Nano Mater.* **2020**, *3*, 94–104. [CrossRef]

10. Fernández, B.; Oyarzabal, I.; Fischer-Fodor, E.; MacAvei, S.; Sánchez, I.; Seco, J.M.; Gómez-Ruiz, S.; Rodríguez-Diéguez, A. Multifunctional applications of a dysprosium-based metal-organic chain with single-ion magnet behaviour. *Crystengcomm* **2016**, *18*, 8718–8721. [CrossRef]
11. Ashebr, T.G.; Li, H.; Ying, X.; Li, X.L.; Zhao, C.; Liu, S.; Tang, J. Emerging Trends on Designing High-Performance Dysprosium(III) Single-Molecule Magnets. *ACS Mater. Lett.* **2022**, *4*, 307–319. [CrossRef]
12. Sessoli, R.; Tsai, H.; Schake, A.R.; Wang, S.; Vincent, J.B.; Foiling, K.; Gatteschi, D.; Christou, G.; Hendrickson, D.N. High-Spin Molecules [Mn12012(02CR)16(H20)4]. *J.Am.Chem. Soc.* **1993**, *115*, 1804–1816. [CrossRef]
13. Zhu, Z.; Guo, M.; Li, X.L.; Tang, J. Molecular magnetism of lanthanide: Advances and perspectives. *Coord. Chem. Rev.* **2019**, *378*, 350–364. [CrossRef]
14. Zhang, P.; Guo, Y.N.; Tang, J. Recent advances in dysprosium-based single molecule magnets: Structural overview and synthetic strategies. *Coord. Chem. Rev.* **2013**, *257*, 1728–1763. [CrossRef]
15. Ungur, L.; Chibotaru, L.F. Strategies toward High-Temperature Lanthanide-Based Single-Molecule Magnets. *Inorg. Chem.* **2016**, *55*, 10043–10056. [CrossRef]
16. Benmansour, S.; Pintado-Zaldo, C.; Martínez-Ponce, J.; Hernández-Paredes, A.; Valero-Martínez, A.; Gómez-Benmansour, M.; Gómez-García, C.J. The Versatility of Ethylene Glycol to Tune the Dimensionality and Magnetic Properties in DyIII-Anilato-Based Single-Ion Magnets. *Cryst. Growth Des.* **2023**, *23*, 1269–1280. [CrossRef]
17. Espallargas, G.M.; Coronado, E. Magnetic functionalities in MOFs: From the framework to the pore. *Chem. Soc. Rev.* **2018**, *47*, 533–557. [CrossRef]
18. Zeng, M.; Ji, S.Y.; Wu, X.R.; Zhang, Y.Q.; Liu, C.M.; Kou, H.Z. Magnetooptical Properties of Lanthanide(III) Metal-Organic Frameworks Based on an Iridium(III) Metalloligand. *Inorg. Chem.* **2022**, *61*, 3097–3102. [CrossRef] [PubMed]
19. Gendron, F.; Pritchard, B.; Bolvin, H.; Autschbach, J. Single-ion 4f element magnetism: An ab-initio look at $Ln(COT)_2^-$. *Dalt. Trans.* **2015**, *44*, 19886–19900. [CrossRef] [PubMed]
20. Baldoví, J.J.; Coronado, E.; Gaita-Ariño, A.; Gamer, C.; Giménez-Marqués, M.; Espallargas, G.M. A SIM-MOF: Three-dimensional organisation of single-ion magnets with anion-exchange capabilities. *Chem. A Eur. J.* **2014**, *20*, 10695–10702. [CrossRef]
21. Topologies, M.O.F.; Stock, N.; Biswas, S. Synthesis of Metal-Organic Frameworks (MOFs): Routes to Various. *Chem. Rev.* **2012**, *2*, 933–969. [CrossRef]
22. Younis, S.A.; Bhardwaj, N.; Bhardwaj, S.K.; Kim, K.H.; Deep, A. Rare earth metal–organic frameworks (RE-MOFs): Synthesis, properties, and biomedical applications. *Coord. Chem. Rev.* **2021**, *429*, 213620. [CrossRef]
23. Safaei, M.; Foroughi, M.M.; Ebrahimpoor, N.; Jahani, S.; Omidi, A.; Khatami, M. A review on metal-organic frameworks: Synthesis and applications. *TrAC Trends Anal. Chem.* **2019**, *118*, 401–425. [CrossRef]
24. Rinehart, J.D.; Long, J.R. Exploiting single-ion anisotropy in the design of f-element single-molecule magnets. *Chem. Sci.* **2011**, *2*, 2078–2085. [CrossRef]
25. Dey, A.; Kalita, P.; Chandrasekhar, V. Lanthanide(III)-Based Single-Ion Magnets. *ACS Omega* **2018**, *3*, 9462–9475. [CrossRef]
26. Liu, J.L.; Chen, Y.C.; Tong, M.L. Symmetry strategies for high performance lanthanide-based single-molecule magnets. *Chem. Soc. Rev.* **2018**, *47*, 2431–2453. [CrossRef]
27. Kalinke, L.H.G.; Cangussu, D.; Mon, M.; Bruno, R.; Tiburcio, E.; Lloret, F.; Armentano, D.; Pardo, E.; Ferrando-Soria, J. Metal-Organic Frameworks as Playgrounds for Reticulate Single-Molecule Magnets. *Inorg. Chem.* **2019**, *58*, 14498–14506. [CrossRef]
28. Gould, C.A.; McClain, K.R.; Reta, D.; Kragskow, J.G.C.; Marchiori, D.A.; Lachman, E.; Choi, E.S.; Analytis, J.G.; Britt, R.D.; Chilton, N.F.; et al. Ultrahard magnetism from mixed-valence dilanthanide complexes with metal-metal bonding. *Science* **2022**, *375*, 198–202. [CrossRef] [PubMed]
29. Tuna, F.; Smith, C.A.; Bodensteiner, M.; Ungur, L.; Chibotaru, L.F.; McInnes, E.J.L.; Winpenny, R.E.P.; Collison, D.; Layfield, R.A. A High Anisotropy Barrier in a Sulfur-Bridged Organodysprosium Single-Molecule Magnet. *Angew. Chem.* **2012**, *124*, 7082–7086. [CrossRef]
30. Zhu, Z.; Li, X.L.; Liu, S.; Tang, J. External stimuli modulate the magnetic relaxation of lanthanide single-molecule magnets. *Inorg. Chem. Front.* **2020**, *7*, 3315–3326. [CrossRef]
31. Ma, Y.J.; Hu, J.X.; De Han, S.; Pan, J.; Li, J.H.; Wang, G.M. Manipulating On/Off Single-Molecule Magnet Behavior in a Dy(III)-Based Photochromic Complex. *J. Am. Chem. Soc.* **2020**, *142*, 2682–2689. [CrossRef]
32. Su, J.; Yuan, S.; Li, J.; Wang, H.Y.; Ge, J.Y.; Drake, H.F.; Leong, C.F.; Yu, F.; D'Alessandro, D.M.; Kurmoo, M.; et al. Rare-Earth Metal Tetrathiafulvalene Carboxylate Frameworks as Redox-Switchable Single-Molecule Magnets. *Chem. A Eur. J.* **2021**, *27*, 622–627. [CrossRef]
33. Zhang, X.; Vieru, V.; Feng, X.; Liu, J.L.; Zhang, Z.; Na, B.; Shi, W.; Wang, B.W.; Powell, A.K.; Chibotaru, L.F.; et al. Influence of Guest Exchange on the Magnetization Dynamics of Dilanthanide Single-Molecule-Magnet Nodes within a Metal-Organic Framework. *Angew. Chem. Int. Ed.* **2015**, *54*, 9861–9865. [CrossRef] [PubMed]
34. Liu, K.; Zhang, X.; Meng, X.; Shi, W.; Cheng, P.; Powell, A.K. Constraining the coordination geometries of lanthanide centers and magnetic building blocks in frameworks: A new strategy for molecular nanomagnets. *Chem. Soc. Rev.* **2016**, *45*, 2423–2439. [CrossRef]
35. Aratani, I.; Horii, Y.; Takajo, D.; Kotani, Y.; Osawa, H.; Kajiwara, T. Construction of a two-dimensional metal-organic framework with perpendicular magnetic anisotropy composed of single-molecule magnets. *J. Mater. Chem. C* **2023**, *11*, 2082–2088. [CrossRef]

36. Lin, P.H.; Burchell, T.J.; Clérac, R.; Murugesu, M. Dinuclear dysprosium(III) single-molecule magnets with a large anisotropic barrier. *Angew. Chem. Int. Ed.* **2008**, *47*, 8848–8851. [CrossRef] [PubMed]
37. Liu, K.; Li, H.; Zhang, X.; Shi, W.; Cheng, P. Constraining and Tuning the Coordination Geometry of a Lanthanide Ion in Metal-Organic Frameworks: Approach toward a Single-Molecule Magnet. *Inorg. Chem.* **2015**, *54*, 10224–10231. [CrossRef] [PubMed]
38. Wang, M.; Meng, X.; Song, F.; He, Y.; Shi, W.; Gao, H.; Tang, J.; Peng, C. Reversible structural transformation induced switchable single-molecule magnet behavior in lanthanide metal-organic frameworks. *Chem. Commun.* **2018**, *54*, 10183–10186. [CrossRef]
39. Xin, Y.; Wang, J.; Zychowicz, M.; Zakrzewski, J.J.; Nakabayashi, K.; Sieklucka, B.; Chorazy, S.; Ohkoshi, S.I. Dehydration-Hydration Switching of Single-Molecule Magnet Behavior and Visible Photoluminescence in a Cyanido-Bridged DyIIICoIII Framework. *J. Am. Chem. Soc.* **2019**, *141*, 18211–18220. [CrossRef]
40. Monni, N.; Baldoví, J.J.; García-López, V.; Oggianu, M.; Cadoni, E.; Quochi, F.; Clemente-León, M.; Mercuri, M.L.; Coronado, E. Reversible tuning of luminescence and magnetism in a structurally flexible erbium–anilato MOF. *Chem. Sci.* **2022**, *13*, 7419–7428. [CrossRef]
41. Xie, L.S.; Skorupskii, G.; Dincă, M. Electrically Conductive Metal-Organic Frameworks. *Chem. Rev.* **2020**, *120*, 8536–8580. [CrossRef] [PubMed]
42. Cador, O.; Le Guennic, B.; Pointillart, F. Electro-activity and magnetic switching in lanthanide-based single-molecule magnets. *Inorg. Chem. Front.* **2019**, *6*, 3398–3417. [CrossRef]
43. Echenique-Errandonea, E.; Mendes, R.F.; Figueira, F.; Choquesillo-Lazarte, D.; Beobide, G.; Cepeda, J.; Ananias, D.; Rodríguez-Diéguez, A.; Paz, F.A.A.; Seco, J.M. Multifunctional Lanthanide-Based Metal-Organic Frameworks Derived from 3-Amino-4-hydroxybenzoate: Single-Molecule Magnet Behavior, Luminescent Properties for Thermometry, and CO2Adsorptive Capacity. *Inorg. Chem.* **2022**, *61*, 12977–12990. [CrossRef]
44. Riehl, J.P.; Richardson, F.S. Circularly Polarized Luminescence Spectroscopy. *Chem. Rev.* **1986**, *86*, 1–16. [CrossRef]
45. Brandt, J.R.; Salerno, F.; Fuchter, M.J. The added value of small-molecule chirality in technological applications. *Nat. Rev. Chem.* **2017**, *1*, 0045. [CrossRef]
46. Zinna, F.; Di Bari, L. Lanthanide Circularly Polarized Luminescence: Bases and Applications. *Chirality* **2015**, *27*, 1–13. [CrossRef] [PubMed]
47. Huizi-Rayo, U.; Zabala-Lekuona, A.; Terenzi, A.; Cruz, C.M.; Cuerva, J.M.; Rodríguez-Diéguez, A.; García, J.A.; Seco, J.M.; Sebastian, E.S.; Cepeda, J. Influence of thermally induced structural transformations on the magnetic and luminescence properties of tartrate-based chiral lanthanide organic-frameworks. *J. Mater. Chem. C* **2020**, *8*, 8243–8256. [CrossRef]
48. Naman, R.; Waldeck, D.H. Chiral-Induced Spin Selectivity Effectct. *J. Phys. Chem. Lett.* **2012**, *3*, 2178–2187. [CrossRef] [PubMed]
49. Naaman, R.; Paltiel, Y.; Waldeck, D.H. Chiral molecules and the electron spin. *Nat. Rev. Chem.* **2019**, *3*, 250–260. [CrossRef]
50. Huizi-Rayo, U.; Gutierrez, J.; Seco, J.M.; Mujica, V.; Diez-Perez, I.; Ugalde, J.M.; Tercjak, A.; Cepeda, J.; Sebastian, E.S. An Ideal Spin Filter: Long-Range, High-Spin Selectivity in Chiral Helicoidal 3-Dimensional Metal Organic Frameworks. *Nano Lett.* **2020**, *20*, 8476–8482. [CrossRef] [PubMed]
51. Demir, S.; Jeon, I.R.; Long, J.R.; Harris, T.D. Radical ligand-containing single-molecule magnets. *Coord. Chem. Rev.* **2015**, *289*, 149–176. [CrossRef]